

The Voetspoor Intrusion, Southern Kaoko Zone, Namibia: Mineralogical, geochemical and isotopic constraints for the origin of a syenitic magma

Barbara Seth^{1,2}, Martin Okrusch¹, Michael Wilde¹ and Karl H. Hoffmann³

¹Mineralogisches Institut, Universität Würzburg, Am Hubland, D-97074 Würzburg, Germany

²Max-Planck-Institut für Chemie (Abteilung Geochemie), Postfach 3060,
D-55020 Mainz, Germany

³Geological Survey of Namibia, P.O. Box 2168, Windhoek, 9000, Namibia

Voetspoor is a small, late-tectonic intrusion that cuts through metaturbidite sequences of the Southern Kaoko Zone in the Pan-African Damara Orogen. Modally, the intrusion is classified as (quartz-) monzonite. However, chemically only the porphyritic margin of the intrusion has a monzonitic composition whereas the main, equigranular part is designated as syenite. This mildly alkaline, metaluminous intrusion is cut by dikes of aplitic leuco-syenite. Predominant minerals are alkali feldspar and plagioclase An₁₁₋₂₆. Most of the amphiboles plot in the edenite field, but some straddle the border to the magnesiohastingsite (pargasite) and hastingsite (ferropargasite) fields. They may contain armoured relics of diopside. The crystallisation age of the Voetspoor Intrusion has been dated by the Pb-Pb single zircon evaporation technique at 530±3 Ma. Hence, the syenite intruded late-tectonically with respect to the major Pan-African deformation phase in this area. A second zircon generation was dated with the vapour digestion technique and revealed an age of 456±20 Ma. This younger age is interpreted as reflecting new zircon growth during a separate hydrothermal event. Isotopic compositions of the syenites are characterised by moderate initial ϵ_{Nd} values (-3.9 to -4.9) and relatively low initial $^{87}Sr/^{86}Sr$ ratios (0.70586 to 0.70610). These signatures, together with trace element and REE characteristics, are interpreted as reflecting the nature of an enriched lithospheric mantle source rather than significant crustal contamination. The enrichment of this part of the mantle from which the syenitic magma was derived may be the result of subduction processes which are significantly older than the crystallisation age of the Voetspoor Intrusion. The ascent of the syenitic magma might be related to deep-reaching fault zones that formed during a late-stage extension in an orogenic triple junction.

Introduction

Syenites of upper mantle derivation play an important role in the evolution of orogenic belts because they reveal interesting evidence about the nature of the lithospheric mantle. Little is known about the composition of the upper mantle underneath the Pan-African Kaoko and Damara belts since geochemical and isotopic data from mantle-derived, syenitic magmas are still rare (e.g. Jung *et al.*, 1998a). The Voetspoor Intrusion investigated in this study is a small late-tectonic syenite that cuts through weakly metamorphosed turbiditic sediments in the Southern Kaoko Zone (Miller, 1983; see Fig. 1), West Brandberg area.

In the region of the Voetspoor Intrusion, the Kaoko Belt merges with the Northern Zone of the Damara Belt (Damara Inland Branch), forming an orogenic triple junction (cf. Coward, 1981, 1983). The age relationship between these two belts is still open to discussion (e.g. Coward, 1981; Miller, 1983; Hartnady *et al.*, 1985; Stanistreet *et al.*, 1991; Dürr and Dingeldey, 1996), hence, radiometric dating of late- to post-tectonic intrusions is a necessary prerequisite to solve this problem.

In this paper, we present new results of Pb-Pb evaporation and U-Pb vapour digestion single-grain dating on zircons from the Voetspoor Intrusion which yield additional constraints on the timing of deformation and magmatism in the Pan-African Kaoko and Damara belts. In addition, geochemical and isotope characteristics of the Voetspoor Intrusion provide evidence on the nature of the source region of the syenite magma. This will contribute to a better understanding of the character of the lithospheric mantle during the Pan-African Orogeny in Namibia.

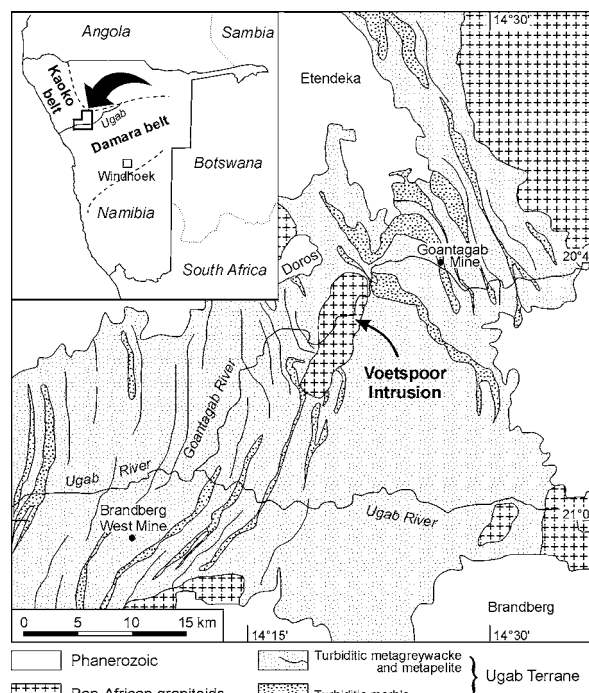


Figure 1. Geological sketch map of the lower Ugab region; modified and simplified after Miller and Grote (1988).

Previous work

So far, the only geochemical and isotopic investigations on Damaran syenites have been undertaken by Jung *et al.* (1998a) in the Okahandja Lineament Zone of the Damara Orogen (zonation after Miller, 1983). These syenites are interpreted as originating from an extremely enriched, lithospheric mantle-derived source and are characterised by low initial ϵ_{Nd} values of -4.3 to -5.5 and relatively high Sr ratios of 0.70706 to 0.70769. These initial values are calculated for an age of 540 Ma, and

thus are comparable with the results of the present study (see below).

Recent geochronological work in the Hoanib-Tomas-Gomatum area (the Purros Terrane of K.-H. Hoffmann, 1987), using conventional U-Pb, Pb-Pb single zircon and SHRIMP methods, has shown that, in the *Kaoko Belt*, two discrete events of widespread granitoid plutonism, at about 650 and between 580 and 552 Ma, can be distinguished (Seth *et al.*, 1998; Seth, 1999). Franz *et al.* (1999) interpret these magmatic phases as being related to the peaks of two different metamorphic events within the Pan-African Orogeny. For the *southern Kaoko Zone*, radiometric age dating is still scarce. A conventional U-Pb zircon age of 577 ± 20 Ma recorded for a post-tectonic granite, about 16 km north of the Huab River Mouth (Miller and Burger, 1983) conforms to the younger phase of plutonic activity in the Kaoko Belt. A similar age of 573 ± 33 Ma (Rb-Sr whole-rock; MSWD 2.51) was recorded by Kröner (1982) for the late- to post-tectonic Voetspoor intrusion. In the *northern Zone* (the Outjo Terrane of K.-H. Hoffmann, 1987) and the *northern Central Zone of the Damara Belt*, zircons from two coarse-grained, porphyritic granitoids ('Salem Granitic Suite') were dated by conventional U-Pb methods yielding upper intercept ages of 589 ± 40 Ma for the Omangambo granite (post- D_2 in the Northern Zone) and 546 ± 30 Ma for the Otjozondjou quartz monzonite (pre- D_2 in the northern Central Zone, corresponding to post- D_2 in the Northern Zone; Miller and Burger, 1983). Rb-Sr whole-rock dating on these plutons gave a conformable, although not very reliable (MSWD 11.5) age of 548 ± 31 Ma (Hawkesworth *et al.*, 1983). A distinctly younger Rb-Sr whole-rock age of 495 ± 15 Ma (MSWD 4.3) was recorded by the same authors for the post-tectonic, alkaline Sorris-Sorris granite which intruded the Omangambo pluton.

Field relations and sampling

The Voetspoor Intrusion, situated on the Farm Goedgenoeg (525), intruded turbiditic rocks (Swart, 1992) of the Ugab Terrane (K.-H. Hoffmann, 1987) in the Southern Kaoko Belt (Miller, 1983). The Ugab Terrane underwent three phases of deformation (Coward, 1981): The first deformation (D_1) produced the dominant structures with westward verging folds during E-W directed compression, whereas the second deformation (D_2) only locally developed crenulations mainly coaxial with F_1 fold hinges. Growth of biotite along S_1 cleavage planes testifies to the peak of metamorphism during this phase of deformation. During D_3 , large-scale, crescent-shaped F_3 interference folds were formed during NNW-SSE compression. As shown in Fig. 1, the Voetspoor Intrusion cuts discordantly through the interlayered and interfolded lithostratigraphic units of the Ugab Terrane. Hence, it post-dates the dominant D_1 structures but was still affected – in parts – by late-stage kinematics (C. Passchier, pers. comm.). Samples of the Voetspoor In-

trusion were taken along a traverse which started about 1.5 m from the margin of the intrusion and ended in its central part. The sample localities are listed in Table 1.

Table 1: Sample localities.

Sample	Topographical coordinates	Rock type modal/chemical
Go-1(a+b)	S20°50.09' E14°21.53'	porphyritic quartz-monzonite/syenodiorite
Go-2	S20°50.03' E14°21.45'	monzonite/syenite
Go-3	S20°50.00' E14°21.45'	monzonite/syenite
Go-4(a+b)	S20°49.96' E14°21.10'	quartz-monzonite/syenite
Go-5	S20°50.06' E14°20.58'	monzonite/syenite
Go-6a	S20°50.06' E14°20.58'	dike of leuco-monzonite/syenite (margin)
Go-6b	S20°50.06' E14°20.58'	dike of leuco-monzonite/syenite (core)

Analytical techniques

For mineral analyses a CAMECA SX 50 microprobe with four independent channels was used. Instrument conditions are 15 kV acceleration potential and 10 nA specimen current. Bulk rock analyses were performed by standard XRF methods using a PHILLIPS PW 1480 spectrometer. FeO was analysed photometrically. The total amount of volatiles was determined by loss on ignition, correcting for the mass gain due to oxidation of Fe^{2+} . The bulk rock analyses are listed in Table 7.

Analyses of Y and the REE, listed in Table 9, were carried out by ICP-AES, at the GeoForschungsZentrum Potsdam, following the prescriptions of Zuleger and Erzinger (1988). Analytical precision is about 5 % relative standard deviation for Y and all REE, except for Pr.

Isotopic measurements for whole-rock Sm-Nd and Rb-Sr (Table 9) were carried out on a Finnigan-MAT 261 mass spectrometer at the Max-Planck-Institut für Chemie (Abteilung Geochemie) in Mainz. For Rb-Sr and Sm-Nd isotopic analyses, sample powders were mixed with a $^{85}Rb/^{84}Sr$ - and a ^{149}Sm - ^{150}Nd -spike and dissolved, in several steps, in concentrated HF, 6N HCl, and 7N HNO_3 . Sr and Rb were separated by standard cation exchange procedures in columns filled with DOWEX AG 50WX12[®] resin, followed by Sm and Nd separation with HDEHP coated teflon columns. For Rb, Sm and Nd measurements Re-double filaments were used, and Sr was loaded with TaF_5 on W-single filaments. $^{87}Sr/^{86}Sr$ fractionation was corrected by normalising the ratios to $^{86}Sr/^{88}Sr = 0.1194$ (Steiger and Jäger, 1977). Six runs of the Sr standard NBS 987 yielded a mean $^{87}Sr/^{86}Sr$ value of 0.710233 ± 31 . The errors for the $^{87}Rb/^{86}Sr$ ratios are better than 1%. The $^{143}Nd/^{144}Nd$ ratios are normalised to $^{146}Nd/^{144}Nd = 0.7219$. The accuracy of the $^{143}Nd/^{144}Nd$ ratio was monitored by analyses of the La Jolla Nd standard, which yielded a value of 0.511852 ± 20 (n=7) during the present study. The uncertainty assigned to the $^{147}Sm/^{144}Nd$ ratios is better than 0.1%.

Zircons were separated from whole-rock samples,

weighing about 5 kg each. Isotopic measurements were carried out on a Finnigan-MAT 261 mass spectrometer using the secondary electron multiplier in peak jumping mode at the Max-Planck-Institut für Chemie (Abteilung Geochemie) in Mainz. The laboratory procedures for *single zircon evaporation* follow Kober (1986, 1987) with slight modifications (Kröner and Todt, 1988; Kröner *et al.*, 1991). No correction was made for mass fractionation of Pb which is 0.3‰ per atomic mass unit (Todt *et al.*, 1996), insignificant for the age range considered in this study. The *vapour digestion technique for single zircons* was developed by Krogh (1978) and Parrish (1987) and modified by Wendt and Todt (1991) and Wendt (1993). The total Pb laboratory blank was about 3 pg. All ratios were corrected for fractionation using the NBS SRM 981 standard as reference (Todt *et al.*, 1996). These fractionation factors scatter at around $3.0 \pm 0.3\%$ per AMU during the period of measurement. All errors are reported at the 2σ level including ratio reproducibility, correction for non-linearity of the secondary electron multiplier and correction for common lead. Regression calculation follows York (1969), and ages and errors are calculated and illustrated in a concordia diagram using the ISOPLOT program of Ludwig (1994). Some initial analyses were highly discordant and the zircons were therefore abraded for several hours using the air abrasion technique of Krogh (1982) leading to more concordant results.

Petrography and mineralogy

Modal composition and rock structure

The Voetspoor intrusive rocks are monzonitic to quartz-monzonitic in modal composition (Table 2). Chemically, however, most of the Voetspoor rocks classify as syenites (Fig. 5). The marginal facies of the Voetspoor Intrusion displays a conspicuous porphyritic texture (sample Go-1). Euhedral to anhedral phenocrysts of K-feldspar, up to about 30 mm long and generally 5-10 mm wide, constitute about 10 vol.% of the rock. They are irregularly distributed in a medium-

grained matrix consisting of subhedral, equant grains of K-feldspar, plagioclase, quartz, and equal portions of partly chloritised amphibole and biotite (Table 2). Subparallel alignment of the phenocrysts parallel to the margin of the pluton is most probably due to magmatic flow. The K-feldspar phenocrysts contain numerous inclusions of plagioclase, more rarely of amphibole and biotite. Therefore, the phenocrysts do not represent an early crystallisation stage in a complex magmatic history, but are due to a low nucleation rate of K-feldspar relative to plagioclase (cf. Hibbard, 1995).

Towards the central part of the Voetspoor Intrusion, K-feldspar phenocrysts gradually become smaller and vanish, giving rise to a medium-grained, equigranular texture, formed by K-feldspar, plagioclase, amphibole and subordinate quartz (Go-2 to -5, Table 2). Small mafic xenoliths of cm-size are locally present (e.g. sample Go-2).

Aplitic leuco-monzonitic dikes cut the Voetspoor Intrusion. They reveal a medium-grained, equigranular texture and consist of subhedral, equant grains of K-feldspar and plagioclase with minor amphibole and quartz.

Individual minerals

Phenocrystic and matrix *K-feldspar* encloses all other minerals, most frequently plagioclase and plagioclase-quartz intergrowths. K-feldspar shows recrystallised margins with formation of bulbous myrmekite (Phillips, 1974). Carlsbad twinning of K-feldspar is widespread. Tartan twinning typical of microcline was observed only in the aplitic sample Go-6b. All K-feldspars are perthitic; braided perthite is most common but patch and vein perthite are also present. Compositional variation of the K-feldspars is relatively small: $Or_{86-92}Ab_{6-13}Ce_{1.4-4.1}An_{<0.2}$ (Table 3, Fig. 2). K-feldspars of sample Go-5 contain areas with high amounts of Ba, conforming to celsian contents of up to 6.4 mol.% (not shown in Table 3). These may be due to local infiltration of Ba-rich hydrothermal fluids during a late stage of the magmatic evolution (Mehnert and Büsch, 1981, 1985) or a separate thermal event (see below).

Anhedral to subhedral *plagioclase* is frequently

Table 2: Modal analyses [vol.%].

Sample	-1	-2	-3	-4	-5	-6	-7
Go				4b	6a	6b	
Quartz	6	2.5	2.5	6	2.5	2	2.5
Alk'feldspar	27	43	46	43	45	45	41
Plagioclase	38	34	30	33	30	49	53
Amphibole	14	16	18	14	15	3.5	2.5
Biotite	12	1.5	1	-	+	+	-
(+Chlorite)							
Clinopyroxene	-	-	-	1	3	-	-
Titanite	1	0.5	+	1	2	+	0.5
Allanite/epidote	0.5	0.5	+	0.5	1	0.5	+
Apatite	+	0.5	0.5	0.5	0.5	+	+
Opaques	0.5	+	+	0.5	1	0.5	0.5
Calcite	+	0.5	1	0.5	+	-	-
Others	0.5	+	0.5	+	+	+	+

- not present, + <0.5

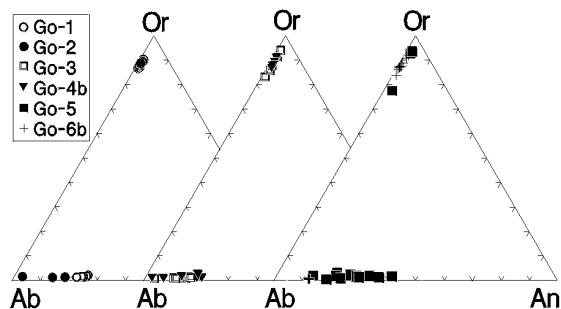


Figure 2. Triangular plot Or - Ab - An [mole.-%] for the analysed K-feldspars and plagioclases.

Table 3: Selected microprobe analyses of K-feldspar and plagioclase [wt.%].

Sample	Go-1a Plag	Go-1a Plag	Go-1b KFS	Go-1b KFS	Go-2 KFS	Go-2 KFS	Go-2 Plag	Go-2 Plag	Go-3 KFS	Go-3 Plag	Go-3 Plag	Go-4b KFS	Go-4b KFS	Go-4b Plag	Go-4b Plag	Go-5 KFS	Go-6b KFS	Go-6b KFS	Go-6b Plag
SiO ₂	61.98	61.68	63.52	62.96	63.87	63.60	65.13	63.63	63.01	64.21	64.62	63.53	63.59	63.30	63.72	63.56	65.34	64.79	65.24
Al ₂ O ₃	23.71	23.87	18.77	19.07	18.81	18.66	22.62	23.07	18.99	21.74	22.21	19.47	19.03	22.62	22.49	19.01	18.72	19.05	22.67
FeO	0.17	0.18	0.07	0.11	0.10	0.06	0.07	0.08	0.05	0.18	0.11	0.00	0.11	0.18	0.09	0.11	0.07	0.08	0.03
MgO	0.00	0.00	0.02	0.00	0.01	0.00	0.00	0.00	0.00	0.00	0.02	0.00	0.00	0.00	0.00	0.00	0.02	0.00	0.01
CaO	5.13	5.36	0.00	0.01	0.00	0.01	2.96	3.83	0.03	2.83	2.71	0.00	0.00	4.14	3.51	0.76	0.00	0.00	2.75
BaO	0.04	0.00	1.33	1.46	0.75	0.78	0.00	0.00	1.86	0.01	0.07	1.71	0.87	0.00	0.07	0.87	1.04	1.16	0.00
Na ₂ O	8.60	8.38	1.14	1.23	1.08	1.10	9.80	9.41	1.22	9.93	10.13	1.17	0.91	9.27	9.53	0.84	1.14	1.13	10.71
K ₂ O	0.25	0.30	14.67	14.32	14.69	14.47	0.13	0.20	14.14	0.21	0.21	14.44	14.63	0.20	0.19	14.88	14.24	14.54	0.17
Total	99.88	99.77	99.52	99.16	99.31	98.68	100.71	100.22	99.30	99.11	100.08	100.32	99.13	99.71	99.60	100.03	100.55	100.75	101.58
Number of cations based on 8 O																			
Si	2.75	2.75	2.97	2.95	2.97	2.98	2.85	2.81	2.96	2.86	2.85	2.95	2.97	2.81	2.83	2.98	3.00	2.98	2.84
Al	1.24	1.25	1.03	1.05	1.03	1.03	1.17	1.20	1.05	1.14	1.15	1.06	1.05	1.18	1.18	1.04	1.01	1.03	1.16
Fe ²⁺	0.01	0.01	0.00	0.00	0.00	0.00	0.00	0.00	0.00	0.01	0.00	0.00	0.00	0.01	0.00	0.00	0.00	0.00	0.00
Mg	0.00	0.00	0.00	0.00	0.00	0.00	0.00	0.00	0.00	0.00	0.00	0.00	0.00	0.00	0.00	0.00	0.00	0.00	0.00
Ca	0.24	0.26	0.00	0.00	0.00	0.00	0.14	0.18	0.00	0.14	0.13	0.00	0.00	0.20	0.17	0.00	0.00	0.00	0.13
Ba	0.00	0.00	0.02	0.03	0.01	0.01	0.00	0.00	0.03	0.00	0.00	0.03	0.02	0.00	0.00	0.02	0.02	0.02	0.00
Na	0.74	0.72	0.10	0.11	0.10	0.10	0.83	0.80	0.11	0.86	0.87	0.11	0.08	0.80	0.82	0.08	0.10	0.10	0.90
K	0.01	0.02	0.87	0.86	0.87	0.86	0.01	0.01	0.85	0.01	0.01	0.85	0.87	0.01	0.01	0.88	0.83	0.85	0.01
Total	5.00	5.00	5.01	5.01	5.00	4.99	4.99	5.00	5.00	5.01	5.01	5.00	4.99	5.00	5.00	4.98	4.97	4.98	5.04
End member																			
An	24.45	25.66	0.00	0.06	0.07	0.00	14.17	18.18	0.11	13.46	12.75	0.00	0.00	19.59	16.80	0.00	0.00	0.00	12.30
Ab	74.09	72.62	10.29	11.20	9.86	10.24	85.08	80.70	11.16	85.35	85.97	10.63	8.45	79.27	82.01	7.77	10.61	10.35	86.77
Or	1.39	1.73	87.28	86.04	88.68	88.30	0.76	1.12	85.28	1.17	1.16	86.23	89.90	1.14	1.08	90.60	87.43	87.51	0.93
Ce	0.07	0.00	2.43	2.70	1.39	1.46	0.00	0.00	3.45	0.02	0.13	3.14	1.65	0.00	0.11	1.63	1.96	2.15	0.00

twinned after the albite and albite-Carlsbad law, sometimes in combination with the pericline law; patchy antiperthite is present in places. In general, most plagioclase grains are relatively homogeneous and only weakly zoned. Many grains, especially those enclosed in K-feldspar, are surrounded by a thin, clear rim of albite. An contents are mostly in the andesine-oligoclase range (Table 3, Fig. 2). Compositions are An₂₃₋₂₆ in sample Go-1 (unzoned), An₁₁₋₂₀ with rims of An₃₋₇ in samples Go-2, -3, -4 and -6b and An₁₉₋₄₁ with rims of An₁₃ in sample Go-5. The Or contents vary between 0.4 and 1.7 mol.%, and the Ce contents are generally at or below the detection limit.

In nearly all samples investigated, *amphibole* with n_a (greenish yellow) < n_b (bluish to brownish green) ≥ n_y (lighter bluish to brownish green) is the predominant mafic phase. The anhedral or subhedral, often twinned crystals may contain inclusions of clinopyroxene, biotite, accessories, and secondary epidote. The amphibole rims are partly replaced by secondary chlorite. Most grains display a patchy or zonal colour distribution, where brownish-green tints tend to be in the central parts and bluish-green ones in marginal parts of the crystal. The composition of the amphiboles is relatively uniform with (Na+K)A 0.56-0.87, Ti 0.07-0.25 per formula unit (p.f.u.), Si 6.40-6.79 p.f.u. and XMg 0.47-0.57 (Table 4). With few exceptions, the Fe³⁺[VI] content, estimated by the midpoint method of Papike *et al.* (1974), is generally higher than Al[VI]. Most amphiboles plot in the edenite field, but some straddle the border to the magnesiohastingsite (pargasite) and hastingsite (ferropargasite) fields (Fig. 3).

Biotite with n_a (yellow) < n_b ≡ n_y (dark greenish brown) is an important mafic phase only in the porphyritic sample Go-1 (Table 2). The biotite flakes are often

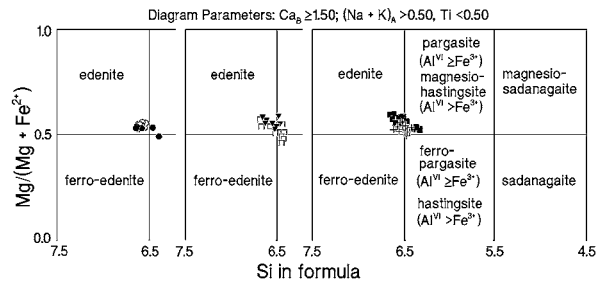


Figure 3. Plot of analysed amphiboles in the diagram Si p.f.u. vs. Mg/(Mg+Fe²⁺) after Leake *et al.* (1997). Symbols as in Figure 2.

bent and partly replaced by green Fe-Mg pycnochlorite or invaded, along the (001) cleavage, by calcite veins. The biotite compositions vary considerably between individual samples (Table 5):

Go-1: X_{Mg} (= Mg/(Mg+Fe^{tot})) 0.52-0.56, total Al 2.49-2.60 p.f.u., Ti 0.18-0.35 p.f.u.;

Go-3: X_{Mg} 0.62-0.63, total Al 2.22-2.26 p.f.u., Ti

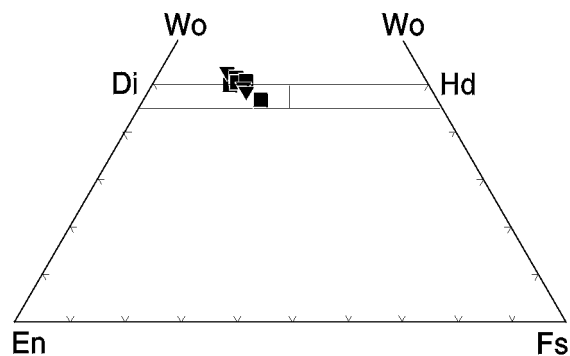


Figure 4. Plot of analysed clinopyroxenes in the pyroxene quadrilateral Di - Hd - En - Fs with demarcation lines after Morimoto *et al.* (1988). Symbols as in Figure 2.

Table 4: Selected microprobe analyses of amphiboles [wt.%].

Sample	Go-1a	Go-1a	Go-1a	Go-1b	Go-1b	Go-2	Go-2	Go-2	Go-3	Go-3	Go-3	Go-4b	Go-4b	Go-4b	Go-5	Go-5	Go-5	Go-6b	Go-6b
SiO ₂	43.05	42.82	43.24	42.82	43.27	41.89	42.35	43.74	42.88	42.06	41.92	42.53	42.53	43.55	42.95	44.57	45.70	44.15	44.61
TiO ₂	1.55	1.12	1.55	1.12	1.55	1.87	1.37	0.82	1.90	2.39	1.92	1.78	2.04	1.39	1.35	1.25	1.26	1.56	0.81
Al ₂ O ₃	8.48	9.05	8.58	9.05	8.45	9.67	9.03	8.41	8.93	9.37	9.13	8.60	8.69	8.15	9.23	8.32	7.60	8.49	8.13
Cr ₂ O ₃	0.06	0.04	0.00	0.04	0.05	0.00	0.00	0.00	0.01	0.03	0.04	0.01	0.00	0.01	0.01	0.02	0.01	0.00	0.00
Fe ₂ O ₃	3.67	2.86	2.61	2.86	2.56	2.62	3.35	3.60	1.77	1.52	2.51	4.25	1.47	1.95	2.63	2.33	1.81	0.66	1.96
FeO	15.05	15.82	15.70	15.82	16.13	17.28	15.83	15.80	17.19	16.86	18.27	13.57	16.27	15.79	15.18	14.02	13.85	16.26	15.85
MnO	0.44	0.49	0.52	0.49	0.45	0.51	0.54	0.43	0.45	0.40	0.49	0.46	0.39	0.41	0.42	0.38	0.38	0.52	0.50
MgO	10.51	10.09	10.45	10.09	10.00	9.29	10.11	10.23	10.09	10.14	8.91	11.00	10.74	11.10	10.96	12.18	12.77	10.84	10.97
CaO	11.97	11.64	11.70	11.64	11.79	11.57	11.71	11.81	11.58	11.45	11.39	11.48	11.43	11.66	11.57	11.52	11.76	11.86	11.92
Na ₂ O	1.39	1.72	1.64	1.72	1.40	1.79	1.87	1.55	2.07	2.09	1.89	1.98	2.20	2.02	1.97	1.91	1.79	1.77	1.75
K ₂ O	1.25	1.27	1.24	1.27	1.17	1.58	1.37	1.20	1.39	1.56	1.54	1.45	1.49	1.35	1.49	1.28	1.21	1.36	1.25
Total	97.42	96.91	97.21	96.91	96.81	98.06	97.52	97.59	98.25	97.85	97.99	97.11	97.24	97.38	97.77	97.78	98.12	97.45	97.73
Number of cations based on 23 O																			
Si	6.55	6.56	6.59	6.56	6.62	6.40	6.47	6.65	6.51	6.41	6.44	6.48	6.50	6.62	6.50	6.67	6.79	6.69	6.74
Ti	0.18	0.13	0.18	0.13	0.18	0.22	0.16	0.09	0.22	0.27	0.22	0.20	0.24	0.16	0.15	0.14	0.14	0.18	0.09
Al	1.52	1.63	1.54	1.63	1.53	1.74	1.63	1.51	1.60	1.68	1.65	1.54	1.57	1.46	1.65	1.47	1.33	1.52	1.45
Cr	0.01	0.00	0.00	0.00	0.01	0.00	0.00	0.00	0.00	0.00	0.01	0.00	0.00	0.00	0.00	0.00	0.00	0.00	0.00
Fe ³⁺	0.42	0.33	0.30	0.33	0.30	0.30	0.39	0.41	0.20	0.17	0.29	0.49	0.17	0.22	0.30	0.26	0.20	0.08	0.22
Fe ²⁺	1.91	2.03	2.00	2.03	2.06	2.21	2.02	2.01	2.18	2.15	2.35	1.73	2.08	2.01	1.92	1.76	1.72	2.06	2.00
Mn	0.06	0.06	0.07	0.06	0.06	0.07	0.07	0.06	0.06	0.05	0.06	0.06	0.05	0.05	0.05	0.05	0.05	0.07	0.06
Mg	2.38	2.30	2.37	2.30	2.28	2.12	2.30	2.32	2.28	2.31	2.04	2.50	2.45	2.52	2.48	2.72	2.83	2.45	2.47
Ca	1.95	1.91	1.91	1.91	1.93	1.89	1.92	1.92	1.88	1.87	1.87	1.87	1.87	1.90	1.88	1.85	1.87	1.92	1.93
Na	0.41	0.51	0.48	0.51	0.42	0.53	0.55	0.46	0.61	0.62	0.56	0.58	0.65	0.60	0.58	0.55	0.51	0.52	0.51
K	0.24	0.25	0.24	0.25	0.23	0.31	0.27	0.23	0.27	0.30	0.28	0.29	0.26	0.29	0.26	0.29	0.25	0.23	0.26
Total	15.63	15.71	15.68	15.71	15.61	15.78	15.77	15.65	15.81	15.84	15.80	15.74	15.87	15.80	15.80	15.72	15.68	15.73	15.71
Occupations																			
T																			
Si	6.55	6.56	6.59	6.56	6.62	6.40	6.47	6.65	6.51	6.41	6.44	6.48	6.50	6.62	6.50	6.67	6.79	6.69	6.74
Al	1.45	1.44	1.41	1.44	1.38	1.60	1.53	1.36	1.49	1.59	1.56	1.52	1.50	1.38	1.50	1.33	1.21	1.31	1.26
Cr	0.00	0.00	0.00	0.00	0.00	0.00	0.00	0.00	0.00	0.00	0.00	0.00	0.00	0.00	0.00	0.00	0.00	0.00	0.00
Fe ³⁺	0.00	0.00	0.00	0.00	0.00	0.00	0.00	0.00	0.00	0.00	0.00	0.00	0.00	0.00	0.00	0.00	0.00	0.00	0.00
Total	8.00	8.00	8.00	8.00	8.00	8.00	8.00	8.00	8.00	8.00	8.00	8.00	8.00	8.00	8.00	8.00	8.00	8.00	8.00
C																			
Ti	0.18	0.13	0.18	0.13	0.18	0.22	0.16	0.09	0.22	0.27	0.22	0.20	0.24	0.16	0.15	0.14	0.14	0.18	0.09
Al	0.07	0.19	0.13	0.19	0.15	0.14	0.10	0.15	0.11	0.10	0.09	0.02	0.07	0.08	0.15	0.14	0.12	0.20	0.18
Cr	0.01	0.00	0.00	0.00	0.01	0.00	0.00	0.00	0.00	0.00	0.01	0.00	0.00	0.00	0.00	0.00	0.00	0.00	0.00
Fe ³⁺	0.42	0.33	0.30	0.33	0.30	0.30	0.39	0.41	0.20	0.17	0.29	0.49	0.17	0.22	0.30	0.26	0.20	0.08	0.22
Fe ²⁺	1.91	2.03	2.00	2.03	2.06	2.21	2.02	2.01	2.18	2.15	2.35	1.73	2.08	2.01	1.92	1.73	1.71	2.06	2.00
Mn	0.03	0.02	0.02	0.02	0.03	0.02	0.03	0.02	0.01	0.00	0.01	0.06	0.00	0.01	0.00	0.00	0.00	0.04	0.03
Mg	2.38	2.30	2.37	2.30	2.28	2.12	2.30	2.32	2.28	2.31	2.04	2.50	2.45	2.52	2.48	2.72	2.83	2.45	2.47
Total	5.00	5.00	5.00	5.00	5.00	5.00	5.00	5.00	5.00	5.00	5.00	5.00	5.00	5.00	5.00	5.00	5.00	5.00	5.00
B																			
Fe ²⁺	0.00	0.00	0.00	0.00	0.00	0.00	0.00	0.00	0.00	0.00	0.00	0.00	0.00	0.00	0.00	0.02	0.01	0.00	0.00
Mn	0.02	0.04	0.04	0.04	0.03	0.05	0.04	0.04	0.05	0.05	0.06	0.00	0.05	0.05	0.05	0.05	0.05	0.03	0.03
Mg	0.00	0.00	0.00	0.00	0.00	0.00	0.00	0.00	0.00	0.00	0.00	0.00	0.00	0.00	0.00	0.00	0.00	0.00	0.00
Ca	1.95	1.91	1.91	1.91	1.93	1.89	1.92	1.92	1.88	1.87	1.87	1.87	1.87	1.90	1.88	1.85	1.87	1.92	1.93
Na	0.03	0.05	0.05	0.05	0.04	0.06	0.05	0.04	0.07	0.08	0.07	0.13	0.08	0.05	0.07	0.08	0.07	0.05	0.04
Total	2.00	2.00	2.00	2.00	2.00	2.00	2.00	2.00	2.00	2.00	2.00	2.00	2.00	2.00	2.00	2.00	2.00	2.00	2.00
A																			
Na	0.39	0.46	0.44	0.46	0.38	0.47	0.51	0.42	0.54	0.54	0.50	0.46	0.58	0.54	0.51	0.47	0.45	0.47	0.47
K	0.24	0.25	0.24	0.25	0.23	0.31	0.27	0.23	0.27	0.30	0.30	0.28	0.29	0.26	0.29	0.25	0.23	0.26	0.24
Total	0.63	0.71	0.68	0.71	0.61	0.78	0.77	0.65	0.81	0.84	0.80	0.74	0.87	0.80	0.80	0.72	0.68	0.73	0.71

0.15-0.16 p.f.u.

The nearly ideal interlayer occupancy of ≥ 1.9 indicates that at least portions of the investigated biotites are relatively unaffected by alteration processes.

In samples Go-4 and -5, diopsidic *clinopyroxene* relics are included in, or intergrown with, amphibole. Clinopyroxene grains display exsolution lamellae, presumably of ortho-pyroxene. The compositions are in the range $Wo_{43.5-46.6}En_{32.1-35.2}Fs_{9.8-16.2}Ac_{3.8-6.8}CaTs_{1.0-2.5}$ (Table 6, Fig. 4).

Common accessory minerals are titanite, epidote, \pm allanite, apatite, zircon, monazite, xenotime, and pyrite,

partly replaced by goethite. Titanite, apatite and zircon occur in the matrix and as inclusions in biotite. Additional secondary alteration products of different silicate minerals are sericite, chlorite, calcite and part of the epidote. Radial aggregates of prehnite, intergrown with calcite, occur in sample Go-6b.

Whole rock geochemistry

Chemical classification

The Voetspoor intrusives are intermediate rocks with

Table 5: Selected microprobe analyses of biotites [wt.%].

Sample	Go-1a	Go-1a	Go-1a	Go-1a	Go-1a	Go-1a	Go-3	Go-3	Go-3	Go-3
SiO ₂	37.09	36.82	36.71	37.53	36.80	36.98	38.74	38.85	38.23	38.67
TiO ₂	2.60	2.80	1.86	1.58	3.00	1.69	1.38	1.37	1.33	1.39
Al ₂ O ₃	13.87	13.93	14.20	14.63	13.80	14.24	12.59	12.43	12.63	12.52
Cr ₂ O ₃	0.08	0.01	0.00	0.03	0.01	0.03	0.00	0.00	0.01	0.02
FeO	19.28	19.63	19.80	18.94	19.82	19.14	16.45	16.35	16.97	16.86
MnO	0.29	0.36	0.31	0.30	0.33	0.35	0.27	0.27	0.24	0.20
MgO	12.48	12.02	12.63	13.33	12.04	13.06	15.31	15.69	15.45	15.57
CaO	0.12	0.38	0.77	0.02	0.15	0.08	0.07	0.07	0.06	0.12
BaO	0.01	0.00	0.00	0.02	0.02	0.00	0.00	0.01	0.01	0.00
Na ₂ O	0.09	0.11	0.12	0.13	0.07	0.08	0.08	0.08	0.05	0.07
K ₂ O	9.81	9.77	9.61	9.83	9.60	9.77	9.91	9.69	9.92	9.79
H ₂ O	3.93	3.92	3.93	3.97	3.92	3.92	3.96	3.96	3.94	3.97
Total	99.62	99.75	99.94	100.25	99.54	99.39	98.77	98.76	98.85	99.15
Number of cations based on 22 O										
Si	5.66	5.63	5.61	5.67	5.64	5.66	5.87	5.88	5.81	5.85
Ti	0.30	0.32	0.21	0.18	0.35	0.19	0.16	0.16	0.15	0.16
Al	2.49	2.51	2.56	2.60	2.49	2.57	2.25	2.22	2.26	2.23
Cr	0.01	0.00	0.00	0.00	0.00	0.00	0.00	0.00	0.00	0.00
Fe	2.46	2.51	2.53	2.39	2.54	2.45	2.09	2.07	2.16	2.13
Mn	0.04	0.05	0.04	0.04	0.04	0.05	0.03	0.03	0.03	0.03
Mg	2.84	2.74	2.88	3.00	2.75	2.98	3.46	3.54	3.50	3.51
Ca	0.02	0.06	0.13	0.00	0.02	0.01	0.01	0.01	0.01	0.02
Ba	0.00	0.00	0.00	0.00	0.00	0.00	0.00	0.00	0.00	0.00
Na	0.03	0.03	0.04	0.04	0.02	0.03	0.02	0.02	0.01	0.02
K	1.91	1.906	1.873	1.893	1.875	1.906	1.916	1.872	1.924	1.888
Total	15.76	15.76	15.86	15.82	15.72	15.83	15.81	15.80	15.87	15.83
X(Fe)	0.46	0.48	0.47	0.44	0.48	0.45	0.38	0.37	0.38	0.38
Si	5.66	5.63	5.61	5.67	5.64	5.66	5.87	5.88	5.81	5.85
Al ^{IV}	2.34	2.37	2.39	2.33	2.37	2.35	2.13	2.12	2.19	2.15
tetr.	8.00	8.00	8.00	8.00	8.00	8.00	8.00	8.00	8.00	8.00
Al ^{VI}	0.16	0.14	0.16	0.27	0.13	0.22	0.12	0.10	0.08	0.08
Cr	0.01	0.00	0.00	0.00	0.00	0.00	0.00	0.00	0.00	0.00
Ti	0.30	0.32	0.21	0.18	0.35	0.19	0.16	0.16	0.15	0.16
Fe ²⁺ tot.	2.46	2.51	2.53	2.39	2.54	2.45	2.09	2.07	2.16	2.13
Mn	0.04	0.05	0.04	0.04	0.04	0.05	0.03	0.03	0.03	0.03
Mg	2.84	2.74	2.88	3.00	2.75	2.98	3.46	3.54	3.50	3.51
okta.	5.80	5.76	5.82	5.88	5.80	5.89	5.86	5.90	5.92	5.90
Ba	0.00	0.00	0.00	0.00	0.00	0.00	0.00	0.00	0.00	0.00
Ca	0.02	0.06	0.13	0.00	0.02	0.01	0.01	0.01	0.01	0.02
Na	0.03	0.03	0.04	0.04	0.02	0.03	0.02	0.02	0.01	0.02
K	1.91	1.91	1.87	1.89	1.88	1.91	1.92	1.87	1.92	1.89
interl.	1.96	2.00	2.03	1.94	1.92	1.95	1.95	1.91	1.95	1.93
Total	15.76	15.76	15.86	15.82	15.72	15.83	15.81	15.80	15.87	15.83

Table 6: Selected microprobe analyses of clinopyroxenes [wt.%].

Sampl e	Go -4b	Go -4b	Go -4b	Go -5	Go -5	Go -5	Go -5	Go -5
SiO ₂	51.32	51.30	51.32	52.37	51.52	52.28	52.44	52.33
TiO ₂	0.17	0.22	0.09	0.00	0.09	0.05	0.02	0.01
Al ₂ O ₃	1.11	1.13	0.98	0.56	0.93	0.48	0.36	0.51
Cr ₂ O ₃	0.17	0.17	0.17	0.01	0.04	0.02	0.02	0.00
Fe ₂ O ₃	3.47	3.61	3.65	2.83	3.10	3.15	3.17	2.84
MgO	10.99	11.67	11.81	12.36	11.56	11.74	12.32	13.11
CaO	23.11	22.85	23.15	23.85	23.54	23.82	24.29	24.27
MnO	0.59	0.56	0.54	0.50	0.47	0.53	0.55	0.48
FeO	7.61	7.10	6.78	6.81	7.49	7.07	6.76	5.45
Na ₂ O	0.88	0.92	0.99	0.74	0.83	0.77	0.54	0.58
K ₂ O	0.03	0.02	0.02	0.02	0.02	0.01	0.01	0.00
Total	99.45	99.55	99.50	100.05	99.59	99.92	100.48	99.58
Numbers of cations based on 6 O								
Si	1.97	1.94	1.94	1.93	1.96	1.97	1.96	1.95
Ti	0.00	0.01	0.00	0.00	0.00	0.00	0.00	0.00
Al	0.05	0.05	0.04	0.02	0.04	0.02	0.02	0.02
Cr	0.01	0.01	0.01	0.00	0.00	0.00	0.00	0.00
Fe ³⁺	0.08	0.10	0.10	0.08	0.08	0.09	0.09	0.09
Fe ²⁺	0.17	0.24	0.22	0.32	0.22	0.24	0.22	0.21
Mn	0.02	0.02	0.02	0.02	0.02	0.02	0.02	0.02
Mg	0.67	0.67	0.67	0.67	0.67	0.66	0.69	0.71
Ca	0.95	0.92	0.94	0.94	0.96	0.96	0.97	0.97
Na	0.07	0.07	0.07	0.05	0.06	0.06	0.04	0.04
K	0.00	0.00	0.00	0.00	0.00	0.00	0.00	0.00
Total	3.99	4.01	4.02	4.04	4.01	4.01	4.01	4.01

silica contents between 55 and 62 wt.% SiO₂, the highest values being recorded for the two aplitic dike samples Go-6a and b. In the multi-cation R1-R2 diagram of La Roche *et al.* (1980), the samples plot between the alkaline and subalkaline trends (Debon and Lemmet, 1999). In terms of their Shand indices, Al₂O₃/(Na₂O+K₂O) vs. Al₂O₃/(CaO+Na₂O+K₂O) [mol.-%] (Maniar and Piccoli, 1989), all Voetspoor samples are metaluminous.

In the TAS diagram (Cox *et al.*, 1979; Wilson, 1989), most Voetspoor samples, including the aplitic dike, fall into the syenite field and sample Go-1 into the monzonite (syenodiorite) field (Fig. 5). The obvious discrepancy with the modal classification is due to the

relatively low An content of plagioclase. However, in this study the chemical classification is preferred.

Calculation of the CIPW norm (Table 7) yields up to 6.5 wt.% quartz (sample Go-1); sample Go-5 is slightly undersaturated with 2.0 wt.% normative olivine. The aplite samples contain only 0.6-0.7 wt.% normative quartz, which corresponds to the low modal values. The total normative feldspar contents are in the range of 72.3-76.4 wt.% for the syenite samples and 92.9-95.8 wt.% for the aplitic dike samples.

Interelement relationships

Judging from calculated correlation coefficients of >|0.80|, Si and Al display negative correlations with Fe, Mg, Ca, Ti, P, V, Zn, Y, Zr and/or Nb, most of the REE and, less distinctly, with Ni. Conversely, Si and Al show a good positive correlation with Na, but not with K. There are negative correlations between Ca and Sr, poor correlations of K vs. Ba and K vs. Rb, and no correlation between Rb and Sr. Na, Sr and Ba show clear negative correlations with Fe, Mn, Mg, Ca, P, Ti, V, Cr, Zn, Y, Zr, Nb, and the REE. The correlation between Cr and Ni is poor. Some of these interelement relationships are plotted in Harker diagrams (Fig. 6) which display linear correlation trends for the analysed syenites. The aplite samples, however, seem to bend this trend

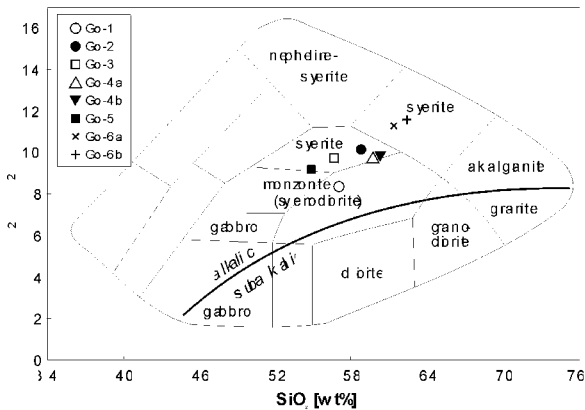


Figure 5. TAS diagram after Cox *et al.* (1979) modified for plutonic rocks after Wilson (1989).

Table 7: Bulk rock analyses of major [wt.%] and trace elements [ppm] and the CIPW norm [wt.%] of syenite samples from the Voetspoor Intrusion.

Sampl	Go-1	Go-2	Go-3	Go-4a	Go-4b	Go-5	Go-6a	Go-6b
SiO ₂	56.93	58.73	56.55	59.98	60.29	54.86	61.37	62.27
TiO ₂	0.85	0.64	0.68	0.62	0.58	0.87	0.34	0.24
Al ₂ O ₃	16.54	16.86	15.93	15.88	16.11	15.48	19.91	20.51
Fe ₂ O ₃	3.23	2.73	2.62	2.10	1.97	2.99	0.19	0.64
FeO	3.15	2.95	3.05	2.55	2.55	3.60	0.80	0.70
MnO	0.13	0.12	0.12	0.10	0.10	0.13	0.03	0.02
MgO	3.33	2.43	2.84	2.34	2.32	3.40	0.70	0.30
CaO	5.54	4.41	5.04	4.70	4.72	6.35	2.93	2.72
Na ₂ O	3.64	4.19	4.08	4.26	4.24	3.98	5.39	5.83
K ₂ O	4.32	5.69	5.41	5.12	5.22	4.89	5.66	5.49
P ₂ O ₅	0.85	0.62	0.68	0.45	0.44	0.82	0.11	0.04
LOI	1.91	1.15	1.14	1.12	1.33	1.06	2.06	1.54
Total	100.42	100.52	98.14	99.22	99.87	98.43	99.49	100.30
Sc	15	<10	11	<10	11	<10	<10	<10
V	128	120	121	107	101	149	43	35
Cr	68	33	30	30	40	38	<10	<10
Co	16	19	25	49	36	22	15	21
Ni	26	13	16	15	13	25	<5	<5
Zn	98	84	87	73	77	103	47	30
Ga	14	22	18	22	23	23	20	19
Rb	132	177	145	162	171	141	169	157
Sr	2035	2309	2437	2278	2393	2306	3457	3587
Y	20	12	26	22	12	32	<8	<8
Zr	515	521	378	305	305	506	248	215
Nb	28	40	36	39	38	33	13	5
Mo	<5	<5	<5	<5	<5	<5	<5	<5
Sn	<15	16	<15	<15	<15	<15	<15	<15
Ba	2980	3430	3577	3146	3375	3416	4430	4263
Pb	28	52	41	48	43	58	56	58
Th	<5	13	20	27	19	16	<5	13
U	11	12	7	11	7	8	6	8
Q	6.49	1.97	1.11	5.38	5.23	0.00	0.73	0.60
C	0.08	0.00	0.00	0.00	0.00	0.00	0.00	0.00
Z	0.10	0.10	0.08	0.06	0.06	0.10	0.05	0.04
Or	25.58	33.70	32.03	30.32	30.92	28.96	33.52	32.51
Ab	30.80	35.45	34.52	36.04	35.87	33.67	45.60	49.33
An	15.96	10.53	9.29	9.19	9.63	10.02	13.80	14.00
Di	0.00	5.22	6.05	6.79	6.67	11.34	1.44	0.83
Hy	10.25	5.92	6.76	4.75	4.92	3.30	1.88	0.76
Ol	0.00	0.00	0.00	0.00	0.00	1.99	0.00	0.00
Mt	4.68	3.96	3.80	3.04	2.86	4.33	0.28	0.93
Cm	0.01	0.01	0.01	0.01	0.01	0.01	0.00	0.00
Il	1.61	1.22	1.29	1.18	1.10	1.65	0.65	0.46
Ap	2.08	1.53	1.68	1.11	1.08	2.00	0.28	0.10

towards lower values of the plotted oxides with increasing SiO₂.

REE geochemistry

The total REE contents range between 704 and 904 ppm for the main intrusion (Go-1 to -5) and between 234 and 276 ppm for the aplitic dike (Go-6a and b; Ta-

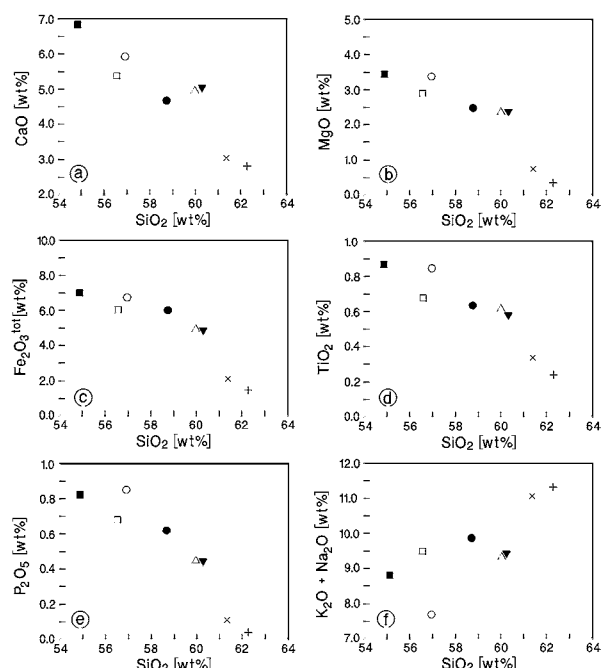


Figure 6. Harker diagrams of wt. % SiO₂ vs. a) CaO, b) MgO, c) Fe₂O₃^{tot}, d) TiO₂, e) P₂O₅, f) Na₂O+K₂O. Symbols as in Figure 5.

ble 8). The chondrite-normalised distribution patterns are characterised by significant enrichment of the LREE over HREE (Fig. 7), with La_N/Yb_N ratios ranging from 35.8 to 59.6. Hence, the distinctive LREE enrichment is responsible for the crystallisation of a considerable amount of LREE-enriched phases like monazite, allanite and apatite. The LREE themselves show a relatively steep slope, with La_N/Sm_N values of 5.0 to 5.9. The fractionation of the HREE, as expressed by the Gd_N/Yb_N ratio, is slightly smaller (3.7 to 4.8) than the LREE fractionation.

The samples Go-1 to -5 show a slight Eu depletion relative to Sm and Gd with Eu/Eu* values of 0.81 to 0.89. For comparison, Eu/Eu* values for the upper

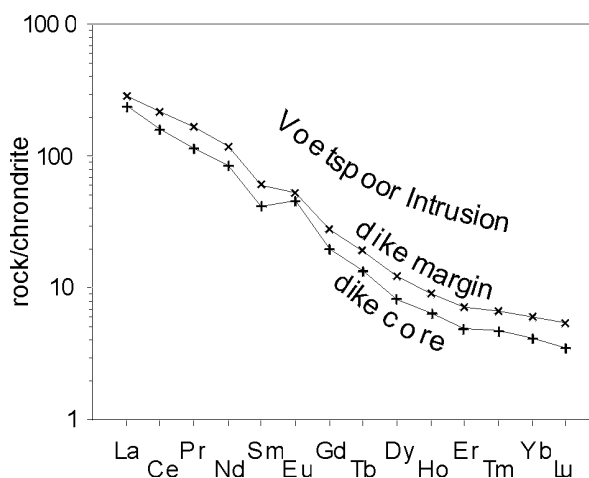


Figure 7. REE patterns of the syenite samples Go-1 to -5 (grey field) and of the aplitic syenite dike samples Go-6a and -6b; chondrite-normalised after Evensen *et al.* (1978).

Table 8: REE and Y concentrations [ppm] of syenite samples from the Voetspoor Intrusion.

Sampl	Go-1	Go-2	Go-3	Go-4a	Go-4b	Go-5	Go-6a	Go-6b
La	175	216	208	186	169	194	70	60
Ce	342	421	399	350	319	381	138	104
Pr	38	44	44	38	35	42	16	11
Nd	137	154	158	133	123	148	57	40
Sm	22	24	25	21	19	24	9.3	6.4
Eu	4.8	5.1	5.4	4.5	4.2	5.5	3.1	2.7
Gd	15	15	15	13	12	15	5.7	4
Tb	1.9	1.8	1.9	1.7	1.5	1.8	0.71	0.5
Dy	8.3	7.5	8	7.2	6.5	7.6	3.1	2.1
Ho	1.5	1.4	1.3	1.2	1.1	1.3	0.51	0.37
Er	3.6	3.2	3.2	2.9	2.7	3.2	1.2	0.81
Tm	0.54	0.49	0.48	0.44	0.41	0.45	0.17	0.12
Yb	3.3	2.8	2.8	2.5	2.3	2.6	1	0.68
Lu	0.5	0.43	0.41	0.36	0.34	0.38	0.14	0.09
Sc	13	8.1	9.3	7.7	7.5	12	2.4	0.75
Y	38	33	35	31	28	33	13	9
Eu/Eu*	0.81	0.82	0.85	0.83	0.85	0.89	1.30	1.63
La _N /Yb _N	35.79	52.07	50.14	50.22	49.60	50.36	47.25	59.56
La _N /Sm _N	5.01	5.67	5.24	5.58	5.60	5.09	4.74	5.90
Gd _N /Yb _N	3.67	4.33	4.33	4.20	4.22	4.66	4.61	4.75

crust are around 0.65 (Taylor and McLennan, 1981). Although the syenite samples contain high amounts of K-feldspar and plagioclase which usually have positive Eu-anomalies (Taylor and McLennan, 1985), these might be compensated for by relatively high contents of minerals with negative Eu-anomalies, like amphibole. In contrast, the aplitic dike samples Go-6a and b have positive Eu-anomalies with Eu/Eu* of 1.30 to 1.63, which can be ascribed to their lower content of accessory phases, higher feldspar/amphibole ratios and, thus, lower contents of LREE.

The chemical differences between the main intrusion and the aplitic dike are also demonstrated by the chondrite-normalised patterns of some REE and other incompatible trace elements (Fig. 8). Compared to the

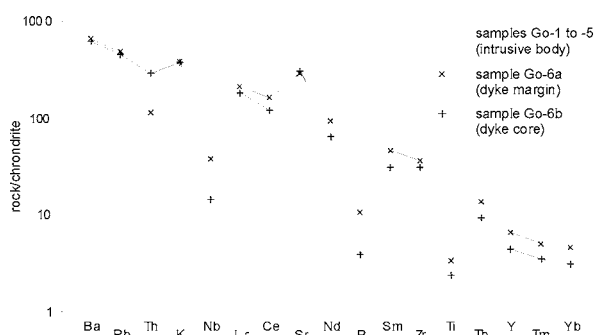


Figure 8. Trace element patterns of the Voetspoor Intrusion samples Go-1 to -5 (grey lines) and the aplitic dike samples Go-6a and -6b; chondrite-normalisation values after Thompson (1982).

Table 9: Sm-Nd and Rb-Sr isotopic data of the syenite samples from the Voetspoor intrusion.

Sample	Sm [ppm]	Nd [ppm]	¹⁴³ Nd/ ¹⁴⁴ Nd		¹⁴⁸ Nd/ ¹⁴⁴ Nd initial	Zircon age [Ma]	ε _{Nd} initial	T _{DMM} [Ga]
			measured*					
Go-1	22	137	0.512072±14	0.0916	0.511753	530	-3.9±0.5	1.2
Go-2	24	154	0.512044±6	0.0850	0.511749	530	-4.0±0.5	1.2
Go-3	25	158	0.512026±10	0.0887	0.511718	530	-4.6±0.5	1.2
Go-4a	21	133	0.512056±15	0.0901	0.511743	530	-4.1±0.5	1.2
Go-4b	19	123	0.512040±8	0.0898	0.511729	530	-4.4±0.5	1.2
Go-5	24	148	0.512032±9	0.0886	0.511725	530	-4.5±0.5	1.2
Go-6a	9.3	57	0.512022±8	0.0919	0.511703	530	-4.9±0.5	1.3
Go-6b	6.4	40	0.512038±11	0.0896	0.511727	530	-4.5±0.5	1.2

Sample	Rb [ppm]	Sr [ppm]	⁸⁷ Sr/ ⁸⁶ Sr		⁸⁷ Rb/ ⁸⁶ Sr initial	Zircon age [Ma]
			measured*			
Go-1	132	2035	0.707441±11	0.1780	0.706096	530
Go-2	177	2309	0.707571±16	0.2209	0.705902	530
Go-3	145	2437	0.707275±10	0.1681	0.706005	530
Go-4a	162	2278	0.707417±8	0.2067	0.705856	530
Go-4b	171	2393	0.707440±9	0.2067	0.705878	530
Go-5	141	2306	0.707338±11	0.1672	0.706075	530
Go-6a	169	3457	0.707125±18	0.1404	0.706064	530
Go-6b	157	3587	0.707031±10	0.1273	0.706069	530

*spike corrected;

main intrusion, the aplitic dike is characterised by distinctly lower contents of Nb, La, Ce, Nd, P, Sm, Ti, Tb, Y, Tm and Yb, and higher contents of Sr and Ba.

Nd- and Sr-isotope geochemical results

The initial ε_{Nd} values of the Voetspoor syenites, including the aplitic dike, range between -3.9 and -4.9 (at 530 Ma, see below). The mean crustal residence ages (after the definition of Arndt and Goldstein, 1987), expressed as TDM (Michard *et al.*, 1985), range between 1.2 and 1.3 Ga. The ¹⁴⁷Sm/¹⁴⁴Nd ratios of all samples are low (0.085-0.092). The low initial ⁸⁷Sr/⁸⁶Sr values of 0.7059 to 0.7061 are higher than the depleted mantle value of ~ 0.7038 at ~ 530 Ma, calculated using uniform-reservoir values of DePaolo and Wasserburg (1976) and Faure (1986). All samples have low ⁸⁷Rb/⁸⁶Sr ratios between 0.127 and 0.221. It should be noted that there is no difference in the Sr and Nd isotope characteristics of the main intrusion and the aplitic dike.

Geochronology

The samples Go-5 and Go-1 were selected for age determination. The zircons from *sample Go-5* are clear

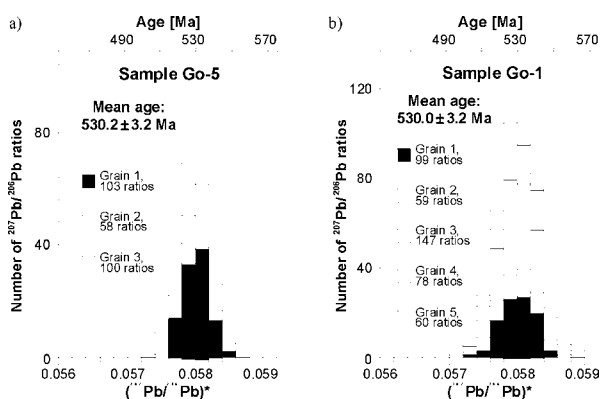


Figure 9. Histograms showing radiogenic Pb isotope ratios derived from evaporation (a) of three grains from sample Go-5 and (b) of five grains from sample Go-1; the spectra have been integrated from 261 and 443 ratios, respectively (see also Table 10).

to pinkish, euhedral and long-prismatic (up to 380 μm). Three grains were evaporated individually and yielded almost identical $^{207}\text{Pb}/^{206}\text{Pb}$ ratios that combine to a mean age of 530.2 ± 3.2 Ma (Fig. 9a, Table 10). A fourth grain of sample Go-5 produced a $^{207}\text{Pb}/^{206}\text{Pb}$ evaporation age of 541.3 ± 7.0 Ma (Table 10) probably indicating some xenocrystic core material in this zircon.

Sample Go-1 contains zircons of two discrete types distinctive in size, colour and morphology. The first type comprises large (250-400 μm), clear to light yellow or pinkish, euhedral and long-prismatic grains which resemble the zircons of sample Go-5, whereas the second type is represented by smaller (< 120 μm), very clear, euhedral and isometric zircon grains. Five grains of the first, larger zircon type were evaporated individually and yielded a combined mean $^{207}\text{Pb}/^{206}\text{Pb}$ age of 530.0 ± 3.2 Ma (Fig. 9b) corresponding exactly to the evaporation age of sample Go-5 (Table 10). Unfortunately, the smaller zircons of the second type did not yield reliable results with the single-zircon evaporation technique, because they are too low in radiogenic Pb.

Therefore, two single-grain U-Pb analyses of the second zircon type in sample Go-1 were carried out by vapour digestion (Table 11). The results are almost concordant but reveal relatively large error ellipses (Fig. 10). However, if the lower intercept is forced through zero, these points define a discordia with high probability (MSWD = 0.00072) and an upper intercept age of 456 ± 20 Ma.

The age of 530 ± 3 Ma is interpreted as the crystallisation age of the Voetspoor Intrusion since the corresponding zircon grains show morphologies typical for

magmatic growth. We regard this date as more reliable than the Rb-Sr whole-rock isochron age of 573 ± 33 Ma (MSWD = 2.51) determined by Kröner (1982). The younger age of 456 ± 20 Ma was obtained from a different type of zircon that still displays an igneous morphology. Since the data points are almost concordant, we interpret this zircon type as belonging to a second zircon generation. The growth of this later generation

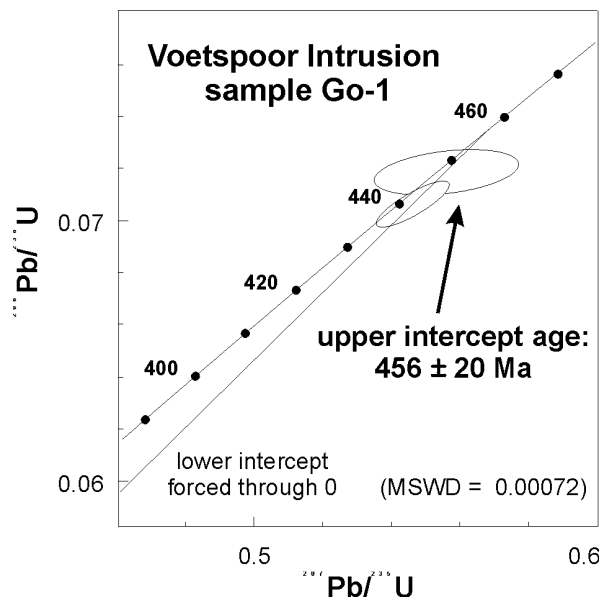


Figure 10. Concordia diagram showing U-Pb isotopic results for vapour digestion analysis of single zircons from syenite sample Go-1 from the Voetspoor Intrusion (for analytical data see Table 11); error ellipses for each analysis are based on 2σ errors.

Table 10: Isotopic data from single grain zircon evaporation from samples Go-1 and Go-5.

sample	Zircon colour and	Grain n	Mass scans	Evaporation on	Mean $^{207}\text{Pb}/^{206}\text{Pb}$ ratio ² and 2- σ m	$^{207}\text{Pb}/^{206}\text{Pb}$ age
Go-1	clear to light yellow, long-prismatic, euhedral	1	99	1585	0.058005 ± 48	529.9 ± 1.8
		2	59	1555	0.058020 ± 107	530.5 ± 4.1
		3	147	1600	0.057995 ± 41	529.6 ± 1.6
		4	78	1585	0.057994 ± 57	529.5 ± 2.2
		5	60	1601	0.058036 ± 150	531.1 ± 5.7
mean of 5		1-5	443	0.058006 ± 32^3	530.0 ± 3.2	
Go-5	clear to pinkish, long-prismatic, euhedral	1	103	1550	0.058012 ± 34	530.2 ± 1.3
		2	58	1556	0.058020 ± 55	530.5 ± 2.1
		3	100	1585	0.058003 ± 69	529.9 ± 2.6
		4	32	1600	0.058307 ± 188	541.3 ± 7.0
mean of 3		1-3	261	0.058010 ± 32^3	530.2 ± 3.2	

¹Number of $^{207}\text{Pb}/^{206}\text{Pb}$ ratios evaluated for age assessment. ²Observed mean ratio corrected for non-radiogenic Pb where necessary. Errors based on uncertainties in counting statistics. ³Correction after internal standard with 2σ error of 0.000085.

Table 11: U and Pb analytical data for vapour digestion single zircon analysis from sample Go-1.

Sample	Grain size [μm]	$^{207}\text{Pb}/^{206}\text{Pb}$ $^{206}\text{Pb}/^{204}\text{Pb}$		Atomic ratios ^b			Apparent ages [Ma]			
		(measured) ^a	(measured) ^a	U/Pb ^c	$^{206}\text{Pb}/^{238}\text{U}$	$^{207}\text{Pb}/^{235}\text{U}$	$^{207}\text{Pb}/^{206}\text{Pb}$	$^{206}\text{Pb}/^{238}\text{U}$	$^{207}\text{Pb}/^{235}\text{U}$	$^{207}\text{Pb}/^{206}\text{Pb}$
Go-1/1	100-120	0.07907 \pm 62	631 \pm 15	10.77	0.0719 \pm 7	0.556 \pm 17	0.05612 \pm 139	447	449	456.9 \pm 54.8
Go-1/2	100-120	0.07321 \pm 14	846 \pm 8	10.62	0.0706 \pm 7	0.546 \pm 9	0.05609 \pm 41	440	443	456.0 \pm 16.2

^ameasured ratios corrected for mass fractionation; errors are 2σ block mean; ^batomic ratios corrected for blank, spike and common lead (Stacey and Kramers, 1975); errors are 2σ ; ^cratio of U over radiogenic lead; uncertainty $\sim 0.5\%$;

is interpreted as reflecting a separate thermal event during which the Voetspoor Intrusion, or a part of it, was penetrated by hydrothermal fluids.

Discussion and conclusions

Age constraints

The crystallisation age of 530 ± 3 Ma of the Voetspoor Intrusion is distinctly younger than the second phase of syn- to late-tectonic granitoid intrusions from the western Hoanib River area in the central segment of the Kaoko Belt (Seth *et al.*, 1998; Seth, 1999) as well as a post-tectonic granite in the southern Kaoko Zone (Miller and Burger, 1983). According to the geochronological results of Hawkesworth *et al.* (1983) and Miller and Burger (1983), the late- to post-tectonic granitoids in the Northern Zone of the Damara Belt are somewhat older than the Voetspoor Intrusion. Field observations have shown that the Voetspoor Intrusion crosscuts the major foliation of the metasedimentary host-rock but was still affected by late-stage deformation (C. Passchier, pers. comm.). Consequently, the emplacement of the Voetspoor syenite was a late event in the kinematic history of the Kaoko Belt and the Northern Zone of the Damara Belt with respect to the main deformation phase and regional metamorphism.

Judging from the U-Pb data, a last significant thermal overprint of the Voetspoor Intrusion took place about 456 ± 20 Ma ago. During this event, an influx of hydrothermal fluids led to the growth of a second zircon generation. We assume that the formation of Barich patches in alkali-feldspars, the chloritisation of biotite and amphibole, the sericitisation of plagioclase and alkali-feldspar, the breakdown of titanite, and the infiltration of calcite veins are at least partly due to this hydrothermal activity.

Petrogenesis of the syenitic magma

The Voetspoor syenite is an alkali-rich, metaluminous and silica-saturated intrusion. REE patterns with high total REE contents and LREE > HREE indicate that the syenite crystallised from a melt with a high solubility of REE-bearing minerals. Hence, the syenite is rich in accessory phases like allanite, apatite and monazite containing high amounts of REE. The enrichment in LREE

may be explained by a low degree of partial melting of an alkali-enriched source rock. The geochemical and isotopic composition of the Voetspoor syenites suggest that fractionation processes in the magma chamber were not extensive and that crustal contamination played only a minor role. Consequently, it is suggested that the compositional characteristics reflect largely the nature of the source area in the upper lithospheric mantle.

Fractional crystallisation

Compositional variations between the main syenite intrusion and the aplitic dike reflect the degree of post-melting fractionation processes. Compared to the main intrusion, the dike is characterised by distinctly lower contents of Nb, La, Ce, Nd, P, Sm, Ti, Tb, Y, Tm and Yb (Fig. 8), matching its lower content of mafic phases, mainly amphibole, and accessory minerals. By contrast, there is a relative enrichment of Sr and Ba in the dike samples which might be explained by feldspar accumulation mainly as a consequence of crystal fractional crystallisation. As a result, the aplitic dike has higher plagioclase contents than the main syenite intrusion (Table 2). However, the slightly negative or lacking Eu anomalies in the main syenite imply that feldspar fractionation is limited. Since there is no correlation between Cr and SiO_2 , the fractionation of clinopyroxene (diopside) plays no significant role. The TiO_2 content decreases with increasing SiO_2 content (Fig. 6) reflecting fractionation of amphibole and titanite. The correlation of P_2O_5 and SiO_2 (Fig. 6) implies significant fractionation of apatite since this is the major phosphorus-bearing phase in the rocks.

The role of crustal contamination

The original compositions of many syenitic magmas emplaced into the continental crust have been modified by reaction with crustal rocks during ascent through, and stagnation within, the crust (e.g. Fowler, 1988). Previous studies on syenites from the Damara belt have suggested that in these rocks crustal contamination is limited (e.g. Jung *et al.*, 1998a). The extreme Sr enrichment of many syenitic rocks makes crustal contamination difficult to verify. However, for the Voetspoor syenite a small amount of crustal contamination might be indicated by the weak positive and negative correla-

tions of the initial Sr isotope ratios with MgO and SiO₂, respectively (Fig. 11a, b), implying a contaminant significantly richer in MgO and poorer in SiO₂ than the syenite magma. Turbiditic country rocks and underlying basement gneisses are the most likely contaminants in this area, but are too low in MgO and too high in SiO₂. It is therefore more likely that these signatures reflect variations in the composition of the source area of the magma. No visible correlation exists between these oxides and the initial ε_{Nd} values indicating that the source was heterogeneous with respect to the Rb/Sr ratios but rather homogeneous with respect to Sm/Nd ratios.

The syenitic magma was not strongly evolved with respect to the Sr isotope system with ⁸⁷Sr/⁸⁶Sr_i around 0.706 which is slightly lower than in syenites from the Okahandja Lineament Zone (e.g. Jung *et al.*, 1998a). Moreover, generally higher Sr_i values were recorded for Pan-African granitic rocks (⁸⁷Sr/⁸⁶Sr₍₅₃₀₎ 0.706 to 0.713) and pre-Pan-African basement gneisses (⁸⁷Sr/⁸⁶Sr₍₅₃₀₎ 0.710 to 0.739) from the Kaoko Belt (Fig. 12; Seth, 1999). The initial ε_{Nd} values of the Voetspoor syenites (-3.9 to -4.9) are much higher than those of nearby Palaeoproterozoic basement gneisses (-20 to -30 at ~ 530 Ma; Seth, 1999; Fig. 13). These isotopic features preclude significant assimilation of older crustal material. Studies on mantle-derived syenites that have undergone crustal contamination show disturbed Sr and Nd isotop-

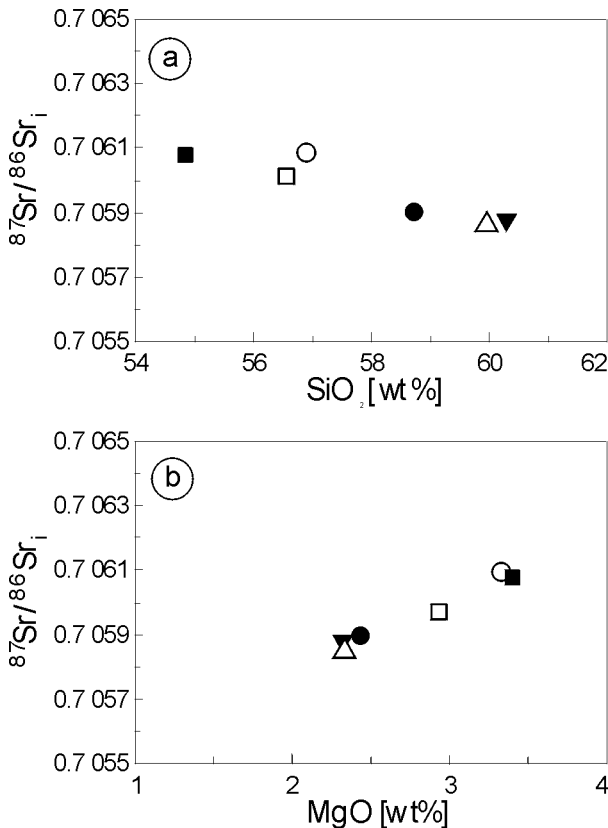


Figure 11. SiO₂ (a) and MgO (b) contents vs. initial ⁸⁷Sr/⁸⁶Sr ratios for the syenite samples of the Voetspoor Intrusion. Symbols as in Figure 5.

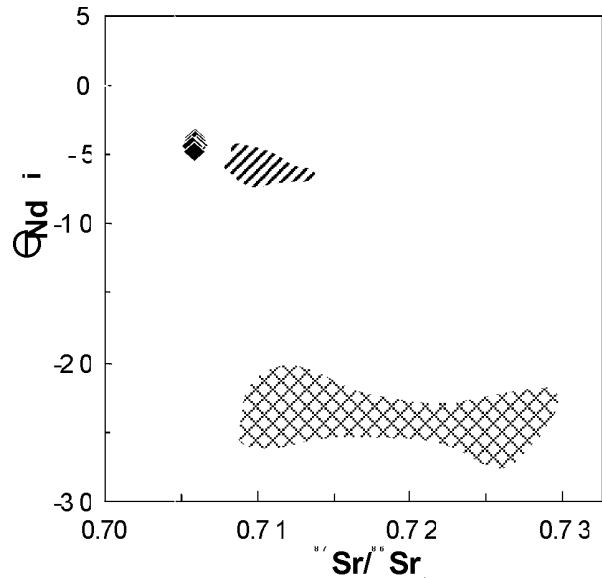


Figure 12. Initial (530 Ma) ε_{Nd} vs. ⁸⁷Sr/⁸⁶Sr_i diagram showing the plots from the Voetspoor syenite samples (black) in comparison to other Pan-African syenites from the Okahandja Lineament Zone (light grey; data from Jung *et al.*, 1998a), to Pan-African granitic rocks from the Kaoko Belt (hatched; data from Seth, 1999) and to pre-Pan-African gneisses from the Kaoko Belt (cross-hatched; data from Seth, 1999).

ic systems (e.g. Fowler, 1988, 1992). Consequently, the geochemical and isotopic features of the Voetspoor syenite are interpreted as reflecting the nature of the mantle source rather than crustal contamination.

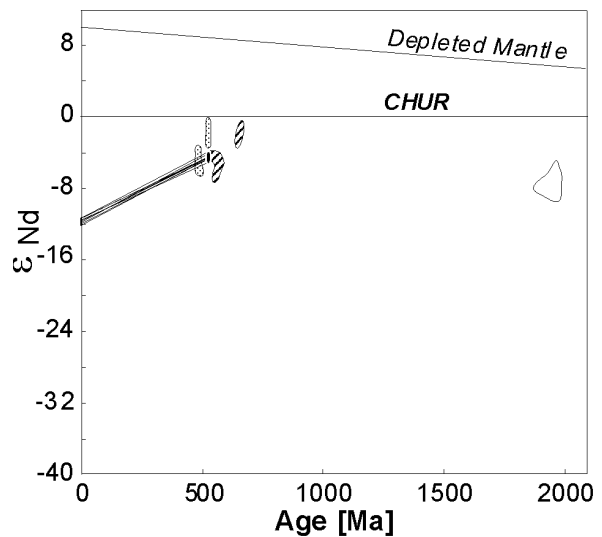


Figure 13. Nd evolution diagram showing fields of initial ε_{Nd} values from the Voetspoor syenite samples obtained in this study (black) in comparison to other Pan-African granitoids from the Kaoko Belt (hatched; data from Seth, 1999) and from the Damara Belt (dotted; data from Jung *et al.*, 1998b) and to pre-Pan-African gneisses from basement inliers in the Kaoko Belt (cross-hatched; data from Seth, 1999); isotopic evolution line for depleted mantle is based on the model proposed by Goldstein *et al.* (1984).

The geochemical features of the Voetspoor Intrusion such as high Ba and Sr contents, negative Nb, P and Ti anomalies (Fig. 8), moderately negative initial ϵ_{Nd} values and relatively low initial $^{87}\text{Sr}/^{86}\text{Sr}$ ratios are significantly different from rift- or hotspot-related syenites (e.g. Baker, 1987; Harris and Grantham, 1993). Most of these features are rather consistent with a subduction zone component. Moreover, the Voetspoor syenite is enriched in terms of incompatible elements like Rb, K, Th and the LREE. The Rb-K relationships of the Voetspoor syenites (Fig. 14) suggest the presence of phlogopite rather than amphibole in the source area conformable with an enriched lithospheric mantle (e.g. Foley, 1992). We conclude that the elemental and isotopic enrichment of the syenites reflects the composition of a phlogopite-bearing upper lithospheric mantle source, from which the magma was extracted about 530 Ma ago. Based on similar isotopic results, Jung *et al.* (1998a) came to the conclusion that the Pan-African syenites in the Okahandja Lineament Zone were derived from a phlogopite-bearing lithospheric mantle source that was enriched by fluids from a subduction zone. By implication, a subduction process also affected the lithospheric mantle beneath the Southern Kaoko Zone, providing the conditions for the formation of the Voetspoor syenite magma. The age of these subduction processes is uncertain, but the syenitic magma evolved from a lithospheric mantle that has been enriched much earlier, most probably in Proterozoic times, since the Nd model ages indicate the involvement of old, enriched components in the source of the syenites. Low $^{147}\text{Sm}/^{144}\text{Nd}$ ratios may be a consequence of small degrees of partial melting but may further indicate enriched upper mantle sources.

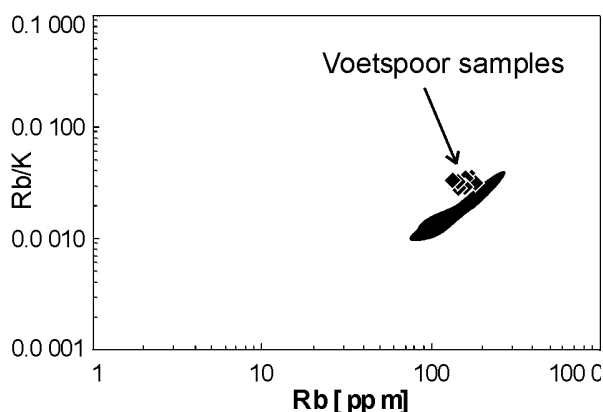


Figure 14. Variation diagram Rb/K vs. Rb plot for the syenite samples of the Voetspoor Intrusion. Phlogopite (dark grey) and amphibole (light grey) composition from Irving and Frey (1984), O'Reilly *et al.* (1991), Adam *et al.* (1993) and Ionov and Hoffmann (1995).

The late-tectonic Voetspoor syenite is situated within an orogenic triple junction (Coward, 1981, 1983) that is characterised by a W-E directed compressional stress field (P.F. Hoffman *et al.*, 1994) during the major deformation phase of the Damara Orogeny. We assume that the emplacement of the syenite took place in an extensional regime that follows shortly after this major compression. These extensional processes, inducing the orogenic collapse, might be responsible for the activation of deep-reaching fault zones which would allow the ascent of magmas from the lithospheric mantle. The Damaran syenites described by Jung *et al.* (1998a) intruded along the Okahandja Lineament, a prominent ENE-striking shear zone, and the authors assume that a change in the stress field which renewed transcurrent movements along lithospheric mega-shear zones was responsible for the intrusion of the Damaran syenites. This might also be true for the Voetspoor Intrusion, and the ascent of the syenitic magma might correspond to deep-reaching fault zones in a late-tectonic extensional regime within the orogenic triple junction.

Acknowledgements

This study was supported by grants from the German Science Foundation (DFG) under grant OK2/59-1. A.W. Hofmann is gratefully acknowledged for providing analytical facilities at the Max-Planck-Institut für Chemie in Mainz. J. Erzinger and E. Kramer from GeoForschungsZentrum Potsdam are thanked for giving access to lab facilities for REE analyses and for their helpful support. We thank U. Schüssler and R. Baur from the Institut für Mineralogie, Universität Würzburg, for their help in microprobe analyses and geochemical lab work, respectively. Detailed support in the isotope lab, valuable suggestions and critical reading of the manuscript by S. Jung helped to improve the paper significantly and are highly appreciated. Thanks are due to C. Miller, R. McG. Miller and A. Nédélec for carefully reviewing the manuscript and to C. Passchier for helpful comments.

References

- Adam, J., Green, T.H. and Sie, S.H. 1993. Proton microprobe determined partitioning of Rb, Sr, Ba, Y, Zr, Nb and Ta between experimentally produced amphiboles and silicate melts with variable F contents. *Chem. Geol.*, **109**, 29-49.
- Arndt, N.T. and Goldstein, S.L. 1987. Use and abuse of crust-formation ages. *Geology*, **15**, 893-895.
- Baker, B.H. 1987. Outline of the petrology of the Kenya rift alkaline province. In: Fitton, J.G. and Upton, B.G.J. (eds.). *Alkaline igneous rocks*. Geol. Soc. Spec. Publ., **30**, 293-311.
- Coward, M.P. 1981. The junction between Pan African

- mobile belts in Namibia: its structural history. *Tectonophysics*, **76**, 59-73.
- Coward, M.P. 1983. The tectonic history of the Damara Belt. *Spec. Publ. Geol. Soc. South Africa*, **11**, 409-421.
- Cox, K.G., Bell, J.D. and Pankhurst, R.J. 1979. *The interpretation of igneous rocks*. Allen & Unwin, London.
- Debon, F. and Lemmet, M. 1999. Evolution of Mg/Fe ratios in Late Variscan plutonic rocks from the external crystalline massifs of the Alps (France, Italy, Switzerland). *J. Petrol.*, **40**, 1151-1185.
- DePaolo, D.J. and Wasserburg, G.J. 1976. Nd isotope variations and petrogenetic models. *Geophys. Res. Lett.*, **3**, 249-252.
- Dürr, S.B. and Dingeldey D.P. 1996. The Kaoko Belt (Namibia), part of a late Neoproterozoic continental-scale strike-slip system. *Geology*, **24**, 503-506.
- Evensen, N.M., Hamilton, P.J. and O'Nions, R.K. 1978. Rare-earth abundances in chondritic meteorites. *Geochim. Cosmochim. Acta*, **42**, 1199-1212.
- Faure, G. 1986. *Principles of isotope geology*. John Wiley & Sons, 589p.
- Foley, S. 1992. Petrological characterization of the source components of potassic magmas: geochemical and experimental constraints. *Lithos*, **28**, 178-204.
- Fowler, M.B. 1988. Elemental evidence for crustal contamination of mantle-derived Caledonian syenite by metasediment anatexis and magma mixing. *Chem. Geol.*, **69**, 1-16.
- Fowler, M.B. 1992. Elemental and O-Sr-Nd isotope geochemistry of the Glen Dessarry syenite, NW Scotland. *J. Geol. Soc. London*, **149**, 209-220.
- Franz, L., Romer, R.L. and Dingeldey, D.P. 1999. Diachronous Pan-African granulite-facies metamorphism (650 Ma and 550 Ma) in the Kaoko belt, NW Namibia. *Eur. J. Mineral.*, **11**, 167-180.
- Goldstein, S.L., O'Nions, R.K. and Hamilton, P.J. 1984. A Sm-Nd isotopic study of atmospheric dust and particulates from major river systems. *Earth Planet. Sci. Lett.*, **70**, 221-236.
- Harris, C. and Grantham, G.H. 1993. Geology and petrogenesis of the Straumsvola nepheline syenite complex, Dronning Maud Land, Antarctica. *Geol. Mag.*, **130**, 513-532.
- Hartnady, C., Joubert, P. and Stowe, C. 1985. Proterozoic crustal evolution in southwestern Africa. *Episodes*, **8**, 236-244.
- Hawkesworth, J.C., Geledhill, A.R., Roddick, J.C., Miller, R.McG. and Kröner, A. 1983. Rb-Sr and ⁴⁰Ar/³⁹Ar studies bearing on models for the thermal evolution of the Damara Belt, Namibia. *Spec. Publ. Geol. Soc. South Africa*, **11**, 323-338.
- Hibbard, M.J. 1995. *Petrography to petrogenesis*. Prentice Hall, Englewood Cliffs, N.J., 587 pp.
- Hippertt, J.F. and Valarelli, J.V. 1998. Myrmekite: constraints on the available models and a new hypothesis for its formation. *Eur. J. Mineral.*, **10**, 317-331.
- Hoffman, P.F., Swart, R., Freyer E.E. and Guowei H. 1994. Geological Excursion Guide -Damara Orogen of Northwest Namibia. Proterozoic Crustal & Metallogenetic Evolution. *Internat. Conf. Geol. Soc. & Geol. Surv. Namibia*, 21-27 Aug 1994, 55 pp.
- Hoffmann, K.-H. 1987. Application of tectonostratigraphic terrane analysis in the Damara Province of central and northern Namibia. *A. L. du Toit Golden Jubilee Conference on Tectonostratigraphic Terrane Analysis. Royal Society and Geological Society of South Africa, Cape Town. Abstract Vol.*, 25-27.
- Ionov, D.A. and Hofmann, A.W. 1995. Nb-Ta-rich mantle amphiboles and micas: implications for subduction-related metasomatic trace element fractionation. *Earth Planet. Sci. Lett.*, **131**, 341-356.
- Irving, A.J. and Frey, F.A. 1984. Trace element abundances in megacrysts and their host basalts: constraints on partition coefficients and megacryst genesis. *Geochim. Cosmochim. Acta*, **48**, 1201-1221.
- Jung, S., Mezger, K. and Hoernes, S. 1998a. Geochemical and isotopic studies of syenites from the Proterozoic Damara belt (Namibia): Implications for the origin of Pan-African syenites. *Min. Mag.*, **62A**, 729-730.
- Jung, S., Mezger, K. and Hoernes, S. 1998b. Petrology and geochemistry of syn- to post-collisional metaluminous A-type granites - a major and trace element and Nd - Sr - Pb -O-isotope study from the Proterozoic Damara Belt, Namibia. *Lithos*, **45**, 147-175.
- Kober, B. 1986. Whole-grain evaporation for ²⁰⁷Pb/²⁰⁶Pb investigation on single zircons using a double-filament thermal ion source. *Contrib. Mineral. Petrol.*, **93**, 482-490.
- Kober, B. 1987. Single-zircon evaporation combined with Pb+ emitter-bedding for ²⁰⁷Pb/²⁰⁶Pb-age investigations using thermal ion mass spectrometry, and implications to zirconology. *Contrib. Mineral. Petrol.*, **96**, 63-71.
- Krogh, T.E. 1978. Vapour transfer for the dissolution of zircons in a multi-sample capsule at high pressures. In: Zartman, R.E. (ed.). 4th International Conference of Geochronology, Cosmochronology, Isotope Geology, 1978, *US Geol. Surv., Open-File Rep.*, **78-701**, 233-234.
- Krogh, T.E. 1982. Improved accuracy of U-Pb zircon ages by the creation of more concordant systems using an air abrasion technique. *Geochim. Cosmochim. Acta*, **46**, 637-649.
- Kröner, A. 1982. Rb-Sr geochronology and tectonic evolution of the Pan-African Damara belt of Namibia, southwestern Africa. *Am. J. Sci.*, **282**, 1471-1507.
- Kröner, A. and Todt, W. 1988. Single zircon dating constraining the maximum age of the Barberton greenstone belt, southern Africa. *J. Geophys. Res.*, **93**, 15329-15337.
- Kröner, A., Byerly, C.R. and Lowe, D.R. 1991. Chronology of early Archean granite-greenstone evolu-

- tion in the Barberton Mountain Land, South Africa, based on precise dating by single zircon evaporation. *Earth Planet. Sci. Lett.*, **103**, 41-54.
- La Roche, H. de, Leterrier, L., Grandclaude, P. and Marchal, M. 1980. A classification of volcanic and plutonic rocks using the R1-R2 diagram and major element analyses. Its relationships with current nomenclature. *Chem. Geol.*, **29**, 183-210.
- Leake, B.E. *et al.* 1997. Nomenclature of amphiboles. Report of the Subcommittee on Amphiboles of the International Mineralogical Association Commission on New Minerals and Mineral Names. *Eur. J. Mineral.*, **9**, 623-651.
- Ludwig, K.R. 1994. ISOPLOT, a plotting and regression program for radiogenic-isotope data, version 2.75. *U.S. Geol. Survey, Open-File Report*, **91-445**, 45 pp.
- Maniar, P.D. and Piccoli, P.M. 1989. Tectonic discrimination of granitoids. *Geol. Soc. America Bull.*, **101**, 635-643.
- Mehnert, K.R. and Büsch, W. 1981. The Ba content of K-feldspar megacrysts in granites: a criterion for their formation. *Neues Jahrb. Mineral. Abhandl.*, **140**, 221-252.
- Mehnert, K.R. and Büsch, W. 1985. The formation of K-feldspar megacrysts in granites, migmatites and augengneisses. *Neues Jahrb. Mineral. Abhandl.*, **151**, 229-259.
- Michard, A., Gurriet, P., Soudant, M. and Albarède, F. 1985. Nd isotopes in French Phanerozoic shales: external vs. internal aspects of crustal evolution. *Geochim. Cosmochim. Acta*, **49**, 601-610.
- Miller, R.McG. 1983. Evolution of the Damara Orogen in South West Africa/Namibia. *Spec. Publ. Geol. Soc. South Africa*, **11**, 431-515.
- Miller, R.McG. and Burger, A.J. 1983. U-Pb zircon ages of members of the Salem Granitic Suite along the northern edge of the central Damara granite belt. *Spec. Publ. Geol. Soc. South Africa*, **11**, 273-280.
- Miller, R.McG. and Grote, W. 1988. Geological map of the Damara Orogen South West Africa/Namibia 1:500 000. *Geol. Surv. Namibia*, Windhoek.
- Morimoto, N. *et al.* 1988. Nomenclature of pyroxenes. Subcommittee on Pyroxenes. Commission on New Minerals and Mineral Names, International Mineralogical Association. *Amer. Mineral.*, **73**, 1123-1133.
- O'Reilly, S.Y., Griffin, W.L. and Ryan, C.G. 1991. Residence of trace elements in metasomatized spinel lherzolite xenoliths: a proton microprobe study. *Contrib. Mineral. Petrol.*, **109**, 98-113.
- Papike, J.J., Cameron, K.L. and Baldwin, K. 1974. Amphiboles and pyroxenes: characterization of other than quadrilateral components and estimates of ferric iron from microprobe data. *Geol. Soc. America Abstr. With Program*, **6**, Boulder, Colorado.
- Parrish, R.R., 1987. An improved micro-capsule for zircon dissolution in U-Pb geochronology. *Isotope Geoscience*, **66**, 99-102.
- Phillips, E.R. 1974. Myrmekite - one hundred years later. *Lithos*, **7**, 181-194.
- Seth, B. 1999. *Crustal evolution of the Kaoko belt, NW Namibia. Geochemical and geochronological study of Archean to Mesoproterozoic basement gneisses and Pan-African migmatites and granitoids*. Dr. rer. nat. thesis, Univ. Würzburg, 120 pp.
- Seth, B., Kröner, A., Mezger, K., Nemchin A.A., Pidgeon, R.T. and Okrusch, M. 1998. Archean and Neoproterozoic magmatic events in the Kaoko belt of NW Namibia and their geodynamic significance. *Precamb. Res.*, **92**, 341-363.
- Stacey, J.S. and Kramers, J.D. 1975. Approximation of terrestrial lead isotope evolution by a two-stage model. *Earth Planet. Sci. Lett.*, **26**, 207-221.
- Stanistreet, I.G., Kukla, P.A. and Henry, G. 1991. Sedimentary basinal responses to a Late Precambrian Wilson Cycle: the Damara Orogen and Nama Foreland, Namibia. *J. Afric. Earth Sci.*, **13**, 141-156.
- Steiger, R.H. and Jäger, E. 1977. Subcommittee on geochronology: Convention on the use of decay constants in geo- and cosmochronology. *Earth Planet. Sci. Lett.*, **36**, 359-362.
- Swart, R. 1992. The sedimentology of the Zerrissene turbiditic system, Damara Orogen, Namibia. *Mem. Geol. Surv. Namibia*, **13**, 54 pp.
- Taylor, S.R. and McLennan, S.M. 1981. The composition and evolution of the continental crust: rare earth element evidence from sedimentary rocks. *Phil. Trans. Royal Soc.*, **A301**, 381-399.
- Taylor, S.R. and McLennan, S.M. 1985. The continental crust: its composition and evolution. Blackwell Scientific Publications, Oxford, 312 pp.
- Thompson, R.N. 1982. British Tertiary volcanic province. *Scott. J. Geol.*, **18**, 49-107.
- Todt, W., Cliff, R.A., Hanser, A. and Hofmann, A.W. 1996. Evaluation of a 202Pb-205Pb double spike for high-precision lead isotope analysis. *Am. Geophys. Union, Geophys. Monogr.*, **95**, 429-437.
- Wendt, J.L. 1993. *Early Archean crustal evolution in Swaziland, southern Africa, as revealed by the combined use of zircon geochronology, Pb-Pb and Sm-Nd systematics*. Ph.D. thesis, Univ. Mainz.
- Wendt, J.I. and Todt, W. 1991. A vapour digestion method for dating single zircons by direct measurement of U and Pb without chemical separation. *Terra Abstracts*, **3**, 507-508.
- Wilson, M. 1989. *Igneous petrogenesis. A global tectonic approach*. Harper Collins, London.
- York, D. 1969. Least-squares fitting of a straight line with correlated errors. *Earth Planet. Sci. Lett.*, **5**, 320-334.
- Zuleger, E. and Erzinger, J. 1988. Determination of the REE and Y in silicate materials with ICP-AES. *Fresenius Zeitschr. Anal. Chem.*, **332**, 140-143.